

Proton-facilitated ammonia excretion by ionocytes of medaka (*Oryzias latipes*) acclimated to seawater

Sian-Tai Liu,¹ Lin Tsung,¹ Jiun-Lin Horng,^{2*} and Li-Yih Lin^{1*}

¹Department of Life Science, National Taiwan Normal University, Taipei, Taiwan; and ²Department of Anatomy, Taipei Medical University, Taipei, Taiwan

Submitted 24 January 2013; accepted in final form 2 May 2013

Liu ST, Tsung L, Horng JL, Lin LY. Proton-facilitated ammonia excretion by ionocytes of medaka (*Oryzias latipes*) acclimated to seawater. *Am J Physiol Regul Integr Comp Physiol* 305: R242–R251, 2013. First published May 15, 2013; doi:10.1152/ajpregu.00047.2013.—The proton-facilitated ammonia excretion is critical for a fish's ability to excrete ammonia in freshwater. However, it remains unclear whether that mechanism is also critical for ammonia excretion in seawater (SW). Using a scanning ion-selective electrode technique (SIET) to measure H⁺ gradients, an acidic boundary layer was detected at the yolk-sac surface of SW-acclimated medaka (*Oryzias latipes*) larvae. The H⁺ gradient detected at the surface of ionocytes was higher than that of keratinocytes in the yolk sac. Treatment with Tricine buffer or EIPA (a NHE inhibitor) reduced the H⁺ gradient and ammonia excretion of larvae. In situ hybridization and immunohistochemistry showed that *slc9a2* (NHE2) and *slc9a3* (NHE3) were expressed in the same SW-type ionocytes. A real-time PCR analysis showed that transfer to SW downregulated branchial mRNA expressions of *slc9a3* and Rhesus glycoproteins (*rhcg1*, *rhcg2*, and *rhbg*) but upregulated that of *slc9a2*. However, *slc9a3*, *rhcg1*, *rhcg2*, and *rhbg* expressions were induced by high ammonia in SW. This study suggests that SW-type ionocytes play a role in acid and ammonia excretion and that the Na⁺/H⁺ exchanger and Rh glycoproteins are involved in the proton-facilitated ammonia excretion mechanism.

mitochondrion-rich cell; gill; fish; embryos; skin

AMMONIA IS A NITROGENOUS PRODUCT of amino acid metabolism. Ammonia excretion in fish is largely accomplished by their gill epithelium, which has a large surface area and a small diffusion distance. Ammonia exists as two distinct chemical species, dissolved ammonia gas (NH₃) and ammonium ions (NH₄⁺). The conventional term, “ammonia,” used in this article refers to both NH₃ and NH₄⁺. In freshwater (FW) fish, it is generally accepted that ammonia excretion occurs by diffusion of non-ionic NH₃ down a favorable gradient across the gill epithelium (7, 11, 35). The excreted NH₃ can be trapped via acid secretion into the unstirred layer of water on gill surfaces. This “acid-trapping” or “proton-facilitated” mechanism maintains a favorable NH₃ gradient across the gill epithelium (35). Although phospholipid membranes are permeable to nonionic NH₃, the existence of NH₃ channels in cell membranes provides an efficient and regulated pathway. In recent years, Rhesus glycoproteins (Rh proteins) in cell membranes of the gill and skin epithelium were found to facilitate ammonia excretion in fishes (11, 12, 39). The human Rh antigen on blood cells has long been associated with blood typing; however, the role of Rh proteins in ammonia transport of erythrocytes and nonerythro-

cytes was discovered in the past decade. The human erythroid RhAG and its nonerythroid homologues, RhBG and RhCG, were demonstrated to function as ammonia transporters or channels (31, 32). In teleosts, Nakada et al. (24) cloned four Rh glycoproteins (Rhag, Rhbg, Rhcg1, and Rhcg2) and localized their distributions in gills of pufferfish (*Takifugu rubripes*). Rhag, Rhbg, and Rhcg2 were localized to lamellar pavement cells, while Rhcg1 was localized to ionocytes (also called mitochondrion-rich cells, MR cells) of gills. In zebrafish, Nakada et al. (23) also identified the four Rh proteins and localized Rhcg1 to the apical membrane of H⁺-ATPase-rich cells (HRCs), an acid-secreting ionocyte (19). Using zebrafish and medaka (*Oryzias latipes*) larvae as models, we investigated the mechanism of ammonia excretion by skin ionocytes. Shih et al. (29) applied a scanning ion-selective technique (SIET) and gene-knockdown technique to show that HRCs play a critical role in ammonia excretion, which is mediated by Rhcg1 and H⁺-ATPase (which secretes H⁺ to facilitate ammonia excretion) in apical membranes. Recently, Shih et al. (30) further showed that the Na⁺/H⁺ exchanger (NHE3b, *slc9a3b*) in the apical membrane of HRCs also contributes to proton-facilitated ammonia excretion, particularly when ambient Na⁺ levels are low. In medaka larvae, Wu et al. (40) found that the coupling of NHE3 and Rhcg1 in apical membranes of ionocytes was involved in ammonia excretion and Na⁺ uptake.

Although the mechanism of ammonia excretion has not been intensively examined in SW fish, it has long been thought that the mechanism in SW fish differs from that in FW fish. Early studies suggested that ionic NH₄⁺ might be excreted via a paracellular pathway in the gill epithelium of SW fish, since the junction of their gill epithelium is leaky in terms of Na⁺ secretion (35). Moreover, proton-facilitated ammonia excretion was questioned in SW fish (34). Because the buffering capability of SW is much higher than that of FW, acid secretion from gills of SW fish might not form an effective acid layer for ammonia trapping. In recent studies, however, expression of Rhcg mRNA in gills and skin was induced by high-ammonia exposure in the mangrove killifish in brackish SW (10). Gill Rhcg1, H⁺-ATPase, and NHE3 mRNAs of pufferfish exposed to high-ammonia (HA)-SW were also elevated (25). Those studies suggested that ammonia excretion in SW fish is also mediated by SW-type ionocytes by a mechanism similar to that of FW fish. However, convincing evidence is still lacking to demonstrate the proton-facilitated ammonia excretion in SW fish.

In this study, we investigated the mechanism of ammonia excretion in SW using the euryhaline medaka as a model. We applied the SIET to measure H⁺ gradients at the skin and ionocyte surfaces of larvae and tested whether the acidic boundary layer forms in SW and whether ammonia excretion is

* J.-L. Horng and L.-Y. Lin contributed equally to this study.

Address for reprint requests and other correspondence: L. Y. Lin, Dept. of Life Science, National Taiwan Normal Univ., Taipei 116, Taiwan (e-mail: linly@ntnu.edu.tw).

associated with acid secretion. We also examined expressions of Rh (*rhcg1*, *rhcg2*, and *rhbq*) and NHE (*slc9a2* and *slc9a3*) transcripts in gills of medaka subjected to SW and high external ammonia challenges to see whether they support the mechanism of ammonia excretion in SW.

MATERIALS AND METHODS

Experimental animals. Mature Japanese medaka (*O. latipes*) was reared in circulating tap water at 27–28°C with a 14:10-h light-dark photoperiod. The females spawned every day, and fertilized egg clusters were collected from the belly of a female and rinsed with tap water to remove the sludge and separate the clusters into single eggs. Medaka embryos usually hatched at 7–8 days postfertilization (dpf), and newly hatched larvae were used for the experiments. During the experiments, larvae were not fed, and the media were changed daily to maintain water quality. The experimental protocols were approved (no. 95013) by the National Taiwan Normal University Animal Care and Utilization Committee.

Acclimation experiments. Solutions for acclimation were prepared by adding salts (Sigma-Aldrich, St. Louis, MO) to redistilled water. Normal fresh water (NW) contained (in mM) 0.5 NaCl, 0.2 CaSO₄, 0.2 MgSO₄, 0.16 KH₂PO₄, and 0.16 K₂HPO₄ (pH 8.0, adjusted with NaOH and HCl). SW was prepared by adding proper amounts of sea salt (Instant Ocean, Aquarium System, Mentor, OH). High-ammonia SW (HA-SW) was prepared by adding 1.25 mM (NH₄)₂SO₄ or 2.5 mM (NH₄)₂SO₄ to SW (pH 8.0, adjusted with NaOH and HCl). For SW or HA-SW acclimation, fertilized eggs were transferred to 20% SW for the first 2 days and then transferred to 30% SW or HA-SW for 5 or 6 days. For the SW or HA-SW acclimation of adult medaka, fish were transferred to 20% SW for 2 days and then transferred to 30% SW or HA-SW for 2 wk. For FW acclimation, fish was transferred to NW for 2 wk. The mortality was usually very low during the acclimation periods.

Measurement of the NH₄⁺ excretion rate. Twenty newly hatched larvae were collected as a sample to measure the NH₄⁺ excretion rate. Larvae were incubated in 1 ml of medium for 1 h at 27–28°C for NH₄⁺ excretion, and then water samples were analyzed with an enzyme-based ammonia assay kit (AA0100, Sigma-Aldrich, St. Louis, MO). The enzyme reacts with only NH₄⁺ but not NH₃. Ideal (linear) FW and SW standard curves were successfully established indicating that the kit can be used to quantify NH₄⁺ in FW and SW. For the assay, 1 ml of working reagent was transferred to a cuvette, 100 μl of water sample was added, and the reaction was recorded following the instruction manual. Excretion rates (micromoles per gram per hour) of larvae were calculated as the difference in concentration in micromole per liter multiplied by the volume of the chamber, divided by the mass of fish and time period.

SIET and measurement of ionic gradients. The SIET was used to measure H⁺ and NH₄⁺ activities at the skin and ionocyte surface of larvae. Glass capillary tubes (no. TW 150-4; World Precision Instruments, Sarasota, FL) were pulled on a Sutter P-97 Flaming Brown pipette puller (Sutter Instruments, San Rafael, CA) into micropipettes with tip diameters of 3–4 μm. These were then baked at 120°C overnight and coated with dimethyl chlorosilane (Sigma-Aldrich) for 30 min. The micropipettes were backfilled with a 1-cm column of electrolytes and frontloaded with a 20–30-μm column of liquid ion-exchange cocktail (Sigma-Aldrich) to create an ion-selective microelectrode (probe). The following ionophore cocktails (and electrolytes) were used: NH₄⁺ ionophore I cocktail B (100 mM NH₄Cl) and H⁺ ionophore I cocktail B (40 mM KH₂PO₄ and 15 mM K₂HPO₄; pH 7). The details of the system were described in previous reports (29, 40). To calibrate the ion-selective probe, the Nernstian property of each microelectrode was measured by placing the microelectrode in a series of standard solutions (0.1, 1, and 10 mM NH₄Cl for the NH₄⁺ probe and pH 6, 7, and 8 for the H⁺ probe; artificial SW standard solutions of different pH values were used for probing the SW

medium). By plotting the voltage output of the probe against log[NH₄⁺] and log[H⁺] values, a linear regression yielded a Nernstian slope of 58.5 ± 0.4 (*n* = 10) for NH₄⁺ and 58.6 ± 0.8 (*n* = 10) for H⁺. The H⁺ probe could specifically sense H⁺ in both FW and SW. However, the NH₄⁺ probe could not specifically sense NH₄⁺ in SW, the NH₄⁺ gradient of specific cells was only measured in FW (NW recording medium).

The SIET was performed at room temperature (26–28°C) in a small plastic recording chamber filled with 2 ml of recording medium. The recording medium for FW fish contained 0.5 mM NaCl, 0.2 mM CaSO₄, 0.2 mM MgSO₄, 300 μM Tricine buffer, and 0.3 mg/l ms222 (Tricaine, Sigma-Aldrich). The recording medium for SW contained 350.9 mM NaCl, 45.7 mM MgCl₂·6H₂O, 24.2 mM Na₂SO₄, 8.9 mM CaCl₂·2H₂O, 7.8 mM KCl, 2 mM NaHCO₃, and 0.3 mg/l ms222. pH values of both the FW and SW recording media were adjusted to 8.0 with HCl and NaOH. Before the measurement, an anesthetized larva was positioned in the center of the chamber with its lateral side contacting the base of the chamber. To measure the H⁺ activity and pH at the surface of the larva, the H⁺-selective probe was moved to the target positions (~10 μm away from the skin surface), voltages were recorded for 1 min, and the median value was used to calculate the H⁺ activity and pH. After recording at the skin surface, the probe was moved away from the skin (~10 mm) to record and calculate the background H⁺ activity and pH. In this study, Δ[H⁺] was used to represent the H⁺ gradient between the target position and background. The gradient reflects the integrated H⁺ activity of skin cells (including keratinocytes and ionocytes) near the target position.

Measurement of H⁺ and NH₄⁺ gradients at specific cells. To record the surface H⁺ (Δ[H⁺]) and NH₄⁺ gradients (Δ[NH₄⁺]) at specific cells, the probe was moved to a position 1–2 μm above the apical membrane of cells. The voltage difference in microvolts was measured by probing orthogonally to the surface at 10-μm intervals. Five replicates of recordings at an ionocyte or keratinocyte were performed, and the median value was used for calculating the Δ[H⁺] of the cell. Voltage differences obtained were converted into ionic gradients by ASET software following previous reports (29, 40). The Δ[H⁺] and Δ[NH₄⁺] of cells reflect the ionic activity, and the apparent flux occurred at the apical membrane of specific cells.

Addition of EIPA and Tricine buffer. NHE inhibitor [5-(*N*-ethyl-*N*-isopropyl) amiloride, EIPA] and Tricine buffer were obtained from Sigma-Aldrich. Stock solutions of EIPA were prepared by dissolving it into DMSO (Sigma-Aldrich). The final concentration of DMSO in the working solutions (including the control group) was 0.1%. Before SIET recording, 10 larvae were incubated in 1 ml of SW medium with EIPA or Tricine for 1 h. After incubation, the larvae were transferred to the SW recording medium that did not contain EIPA. The inhibitor was not added to the recording medium to prevent alteration of the selectivity of the microelectrodes. To analyze the ammonia excretion rate, larvae were incubated in SW medium that contained EIPA or Tricine buffer for 1 h. The pH of the media was adjusted to 8.0.

Preparation of RNA. To obtain a sufficient quantity of RNA, adult medaka gills isolated from six individuals were pooled as one sample. Samples were homogenized in 0.5 ml TRIzol Reagent (Invitrogen, Carlsbad, CA), and DNA contamination was removed with DNase I (Promega, Madison, WI). Total RNA was purified by a MasterPure RNA purification kit (Epicentre Biotechnologies, Madison, WI). The amount of total RNA was determined using a NanoDrop 1000 spectrophotometer (Thermo Scientific, Wilmington, DE). All RNA pellets were stored at –20°C.

Quantitative real-time PCR analysis. For complementary (c)DNA synthesis, 5 μg of total RNA was reverse-transcribed in a final volume of 20 μl containing 0.5 mM dNTPs, 2.5 μM oligo(dT)₂₀, 250 ng of random primers, 5 mM dithiothreitol, 40 units of an RNase inhibitor, and 200 units of SuperScript III RT (Invitrogen, Carlsbad, CA) for 1 h at 50°C, followed by incubation at 70°C for 15 min. The mRNA expression of the target gene was measured by a quantitative real-time PCR (qRT-PCR) with the Roche LightCycler 480 System (Roche

Table 1. Specific primer sets for the qualitative real-time PCR analysis

Name	Primer Sequence
<i>slc9a2</i>	
Forward	5' ATCGTCTGTTGTGCCCTC 3'
Reverse	5' CAGTTCACCTCGTGCTCT 3'
<i>slc9a3</i>	
Forward	5' ATGCCTGATGCTCACTGCT 3'
Reverse	5' GTGTCCGTGCTGCTTCT 3'
<i>rhbg</i>	
Forward	5' CGCTGTGACTCTGGGCAT 3'
Reverse	5' GCTTGTCCGACTCCTCTG 3'
<i>rhcg1</i>	
Forward	5' TGGGAGATGATGGGAAGATAAGC 3'
Reverse	5' GCAATGCTCCATAGGCAATCAA 3'
<i>rhcg2</i>	
Forward	5' CCTGCCGTCTGCTTCTGCTCT 3'
Reverse	5' GCATCTGATTCTCGTCTGCTTACC 3'
<i>rpl7</i>	
Forward	5' GAGATCCGCCTGGCTCGTA 3'
Reverse	5' GGGCTGACTCCGTTGATACCT 3'

Applied Science, Mannheim, Germany). Specific primers for all genes were designed (Table 1) using Primer Premier software (version 5.0; PREMIER Biosoft International, Palo Alto, CA). PCRs contained 3.2 ng of cDNA, 50 nM of each primer, and LightCycler 480 SYBR Green I Master (Roche Applied Science) in a final volume of 10 μ l. All qRT-PCRs were performed as follows: 1 cycle of 50°C for 2 min and 95°C for 10 min, followed by 40 cycles of 95°C for 15 s and 60°C for 1 min (the standard annealing temperature of all primers). PCR products were subjected to a melting-curve analysis, and representative samples were electrophoresed to verify that only a single product was present. Control reactions were conducted with sterile water to determine levels of background and genomic DNA contamination. The standard curve of each gene was confirmed to be in a linear range with ribosomal protein L7 (*rpl7*) as an internal control. The expression level of *rpl7* was not different among FW, SW, and HA-SW groups (data not shown).

RNA probe synthesis. A fragment of *slc9a2* (Ensemble ID: ENSORLG00000012399) was obtained by PCR and inserted into the pGEM-T Easy vector. Specific primers are shown in Table 2. The inserted fragments were amplified with the T7 and SP6 primers by a PCR, and the products were used as templates for in vitro transcription with T7 and SP6 RNA polymerase, respectively (Roche, Penzberg, Germany). Digoxigenin (DIG)-labeled RNA probes were examined using RNA gels and a dot blot assay to confirm their quality and concentrations.

In situ hybridization and immunohistochemistry. Medaka larvae were anesthetized on ice and then fixed with 4% paraformaldehyde in a PBS solution at 4°C overnight. Afterward, samples were washed with diethylpyrocarbonate (DEPC)-PBST (PBS with 0.1% Tween-20) several times (for 10 min each). After a brief rinse with PBST, embryos were refixed with 4% paraformaldehyde for another 20 min. After PBST washing, samples were incubated with hybridization buffer (HyB: 50% formamide, 5 \times SSC, and 0.1% Tween 20) at 65°C for 5 min and with HyB containing 500 μ g/ml yeast tRNA at 65°C for 4 h before hybridization. After overnight hybridization with 100 ng/ml

Table 2. Specific primer sets for the in situ hybridization probe

Name	Primer Sequence
<i>slc9a2</i>	
Forward	5' ACAATGGCTGGCATAGAGGATT 3'
Reverse	5' CGCTAAGGTGGTGACCAAGAC 3'

DIG-labeled antisense or sense RNA probes, embryos were serially washed with 50% formamide-2 \times SSC (at 65°C for 20 min), 2 \times SSC (at 65°C for 10 min), 0.2 \times SSC (at 65°C for 30 min, twice), and PBST at room temperature for 10 min. Afterward, embryos were reacted with an alkaline phosphatase-coupled anti-DIG antibody (diluted 1: 8,000) and then treated with nitro blue tetrazolium and 5-bromo-4-chloro-3-indolyl phosphate for the alkaline phosphatase reaction.

For double staining, in situ hybridized samples were subjected to IHC. After PBS washing, samples were incubated with 3% BSA and 5% normal goat serum for 30 min to block nonspecific binding. Some samples were then incubated overnight at 4°C with an α 5-monoclonal antibody against the α -subunit of the avian Na⁺-K⁺-ATPase (diluted 1: 500) (Developmental Studies Hybridoma Bank, University of Iowa, Ames, IA). Others were incubated with a specific SLC9A3 (NHE3) polyclonal antibody against the C-terminus (VAPSQRAQTRPPLTAG) of the medaka NHE3 protein (diluted 1:1,000) (16). After PBS washing for 20 min, samples were further incubated in goat anti-rabbit IgG conjugated with FITC or goat anti-mouse IgG conjugated with Texas red (Jackson ImmunoResearch Laboratories, West Grove, PA) for 2 h at room temperature. Finally, samples were washed with PBST and stored

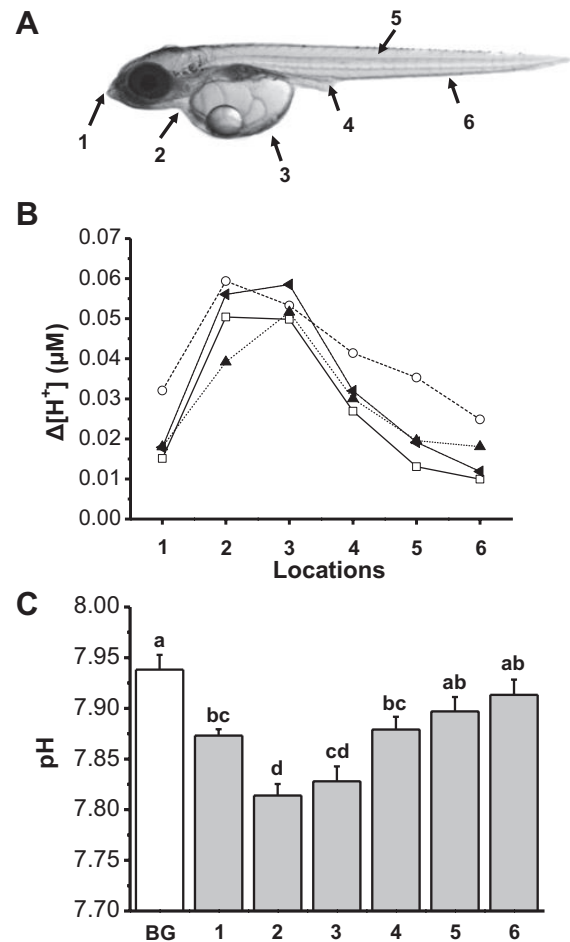


Fig. 1. A: scanning ion-selective electrode technique (SIET) was applied to measure H⁺ activity at the skin surface of seawater (SW)-acclimated medaka larvae. Six spots and a background (BG) were measured: the snout (1), pericardial cavity (2), yolk sac (3), cloaca (4), trunk (5), and tail (6) and 10 mm from the surface (BG). B: $\Delta[H^+]$ measured at six spots of four individuals. C: pH values measured at the six spots and BG ($n = 12$ individuals). a,b,c,d Different letters indicate a significant difference (one-way ANOVA, Tukey's comparison, $P < 0.05$).

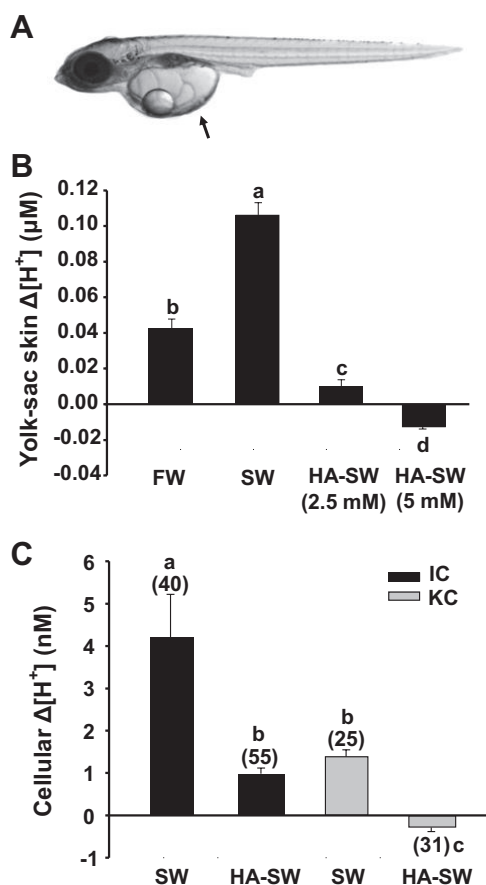


Fig. 2. *A*: arrow indicates the location of the microelectrode. $\Delta[H^+]$ at the yolk sac surface of larvae acclimated to fresh water (FW), seawater (SW), and high ammonia seawater (HA-SW; 2.5 mM and 5 mM) (*B*). Data are presented as the means \pm SE ($n = 12$ individuals). *C*: $\Delta[H^+]$ at the surface of ionocytes (IC) and keratinocytes (KC) in larvae acclimated to SW and 5 mM HA-SW (the number of cells is shown in parentheses). ^{a,b,c,d}Different letters indicate a significant difference (one-way ANOVA, Tukey's comparison, $P < 0.05$).

in PBS at 4°C in a dark box for further examination and analysis. Images were acquired with a Leica TCS-SP5 confocal laser-scanning microscope (Leica Lasertechnik, Heidelberg, Germany).

Statistical analysis. Data are expressed as the means \pm SE (n , number of larvae or ionocytes). Values from each condition were analyzed using one-way ANOVA followed by Tukey's pairwise comparisons. Student's unpaired t -test (two-tailed) was used for simple comparisons of two means. Significance was set at α level of 0.05.

RESULTS

H^+ gradients at the skin surface of larvae acclimated to SW. The surface pH and $\Delta[H^+]$ (H^+ gradient) of SW-acclimated larvae were measured with the SIET. Six spots at the surface of larvae and a background (~ 10 mm away from the larva) were measured, including the snout, pericardial cavity, yolk-sac, cloaca, trunk, and tail (Fig. 1*A*). $\Delta[H^+]$ of the six spots were determined by calculating the difference between the target spot and background (Fig. 1*B*). Figure 1*C* shows pH values of the six spots and background. pH levels of the pericardial cavity and yolk sac were significantly lower (~ 0.12 pH) than that of the background, indicating that acid was being secreted in these areas. Since the $\Delta[H^+]$ was consistently highest at yolk

sac (Fig. 1*B*), yolk sac was selected for H^+ measurement in the following experiments.

H^+ gradients at the yolk sac and ionocyte surfaces of larvae acclimated to FW, SW, and HA-SW. $\Delta[H^+]$ at the yolk sac of larvae acclimated to FW, SW, and HA-SW (SW with 2.5 or 5 mM NH_4^+) for 5 days were measured (Fig. 2*A*; the arrow shows the location of the probe). pH values of the four media were adjusted to the same level (pH 8.0). $\Delta[H^+]$ of the SW group was significantly higher than that of the FW group (Fig. 2*B*). Values of both the 2.5 and 5 mM HA-SW groups were remarkably lower than that of the SW group, and the 5 mM HA-SW group had a negative value (Fig. 2*B*).

Similar results were found when measuring $\Delta[H^+]$ at the surface of specific skin cells (ionocytes and keratinocytes). $\Delta[H^+]$ of cells were measured by probing the H^+ gradient at 10- μm intervals perpendicular to the cell surface. In the SW group, $\Delta[H^+]$ of ionocytes was about three-fold higher than that of keratinocytes (Fig. 2*C*). HA-SW (5 mM NH_4^+) acclimation significantly decreased $\Delta[H^+]$ of both ionocytes and keratinocytes, and $\Delta[H^+]$ of keratinocytes decreased until becoming negative (Fig. 2*C*). Taken together, the decrease of $\Delta[H^+]$ in the HA-SW group suggests that nonionic NH_3 was excreted and alkalized at the skin surface.

NH_4^+ gradients at ionocytes in larvae acclimated to SW and HA-SW. Using the SIET to measure NH_4^+ in SW was not successful because the high-salt condition severely interfered with the selectivity of the NH_4^+ -sensitive microelectrode. Therefore, SIET recordings of the NH_4^+ gradient at the cell

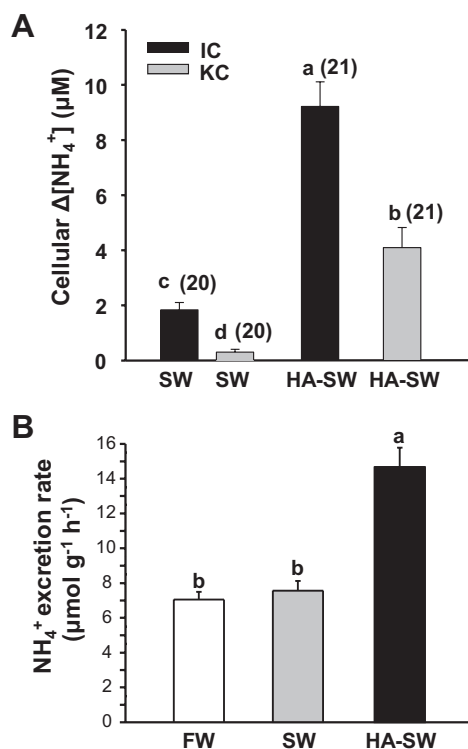


Fig. 3. *A*: $\Delta[NH_4^+]$ at IC and KC in larvae acclimated to SW and HA-SW (5 mM). The larvae were transferred to NW for SIET probing. *B*: NH_4^+ excretion rates of medaka larvae acclimated to FW (pH 8.0) and SW (pH 8.0) and 5 mM HA-SW (pH 8.0). Data are presented as the means \pm SE. The number of cells is shown in parentheses. ^{a,b,c,d}Different letters indicate a significant difference (one-way ANOVA, Tukey's comparison, $P < 0.05$).

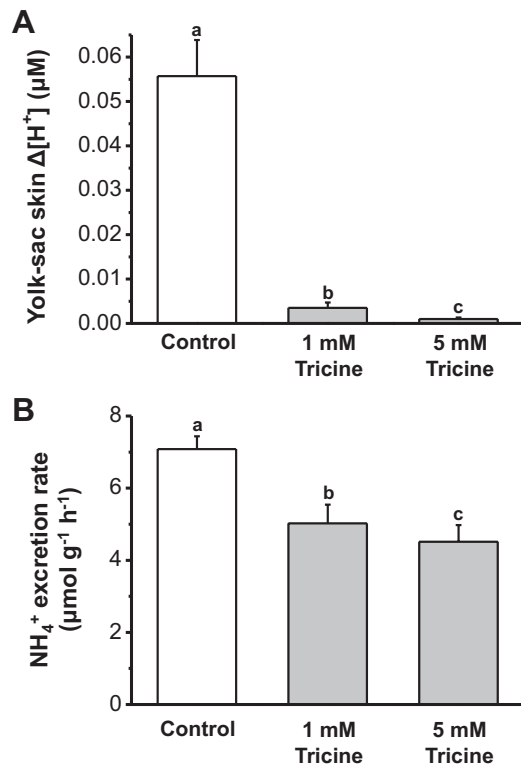


Fig. 4. Effects of Tricine (1 and 5 mM) on $\Delta[\text{H}^+]$ at the yolk-sac surface (A) and ammonia excretion rates (B) of larvae acclimated to seawater. Data are presented as the means \pm SE ($n = 15$ individuals for $\Delta[\text{H}^+]$; $n = 4$ for the ammonia excretion rate). ^{a,b,c}Different letters indicate a significant difference (one-way ANOVA, Tukey's comparison, $P < 0.05$).

surface of SW and HA-SW larvae were conducted in FW medium (NW). Results showed that $\Delta[\text{NH}_4^+]$ at the surface of ionocytes was ~ 2.8 - and 2.2 -fold higher than those of keratinocytes of larvae reared in SW and HA-SW, respectively (Fig. 3A). HA-SW acclimation remarkably increased $\Delta[\text{NH}_4^+]$ of both ionocytes and keratinocytes (Fig. 3A).

In addition, NH_4^+ excretion rates of FW- and SW-acclimated whole larva were analyzed with an enzyme-based ammonia assay and compared. No significant difference was found between the FW and SW groups (Fig. 3B). HA-SW acclimation remarkably increased NH_4^+ excretion rate (Fig. 3B).

Effects of Tricine buffer on the H⁺ gradient at the yolk sac surface and whole-larva NH₄⁺ excretion. To test whether ammonia excretion is facilitated by acid secretion by larval skin, a high concentration of Tricine buffer was added to SW to neutralize acidification of the skin surface. Results showed that the addition of Tricine (1 and 5 mM) effectively eliminated the H⁺ gradient at the yolk sac surface of SW larvae (Fig. 4A). In addition, the NH_4^+ excretion rate of whole larva was suppressed by 35% and 42%, respectively, with 1 and 5 mM Tricine buffer (Fig. 4B).

Effects of EIPA on the H⁺ gradient at the yolk sac surface and whole-larva ammonia excretion. To examine whether the NHE is involved in acid secretion and ammonia excretion in SW larvae, a specific inhibitor (EIPA) was applied to block the NHE (Fig. 5A). Results showed that respective $\Delta[\text{H}^+]$ at the yolk sac surface decreased 19%, 35%, and 49% after exposure to 50, 100, and 200 μM EIPA for 1 h. NH_4^+ excretion rates of

larvae decreased 24% and 34% with 50 and 100 μM EIPA, respectively (Fig. 5B).

Localization of *slc9a2* and *slc9a3* in the yolk sac skin of SW-acclimated larvae. IHC and in situ hybridization were used to localize the *slc9a3* protein (Fig. 6C) and *slc9a2* transcript (Fig. 6A) in larval skin. NKA immunohistochemical staining was used to label ionocytes (Fig. 6B). Images showed that the *slc9a2* transcript was colocalized with NKA signals (Fig. 6, D and E), and the *slc9a3* protein was localized in apical membranes of NKA cells (Fig. 6, D and E). These data demonstrated localization of *slc9a2* and *slc9a3* in the same ionocytes of SW medaka larvae.

Expression levels of *rhb*, *rhcg1*, *rhcg2*, *slc9a2*, and *slc9a3* transcripts in gills of medaka acclimated to FW, SW, and HA-SW. A real-time qPCR was used to examine transcript levels of *rhb*, *rhcg1*, *rhcg2*, *slc9a2* (*NHE2*) and *slc9a3* (*NHE3*) in gills of adult medaka acclimated to FW, SW and HA-SW for 2 wk. Results showed that levels of *rhb*, *rhcg1*, *rhcg2*, and *slc9a3* were significantly lower in the SW than FW group (Fig. 7, A–C, E). In contrast, the level of *slc9a2* was significantly higher in the SW than FW group (Fig. 7D). Comparing the SW and HA-SW groups, levels of *rhcg1*, *rhcg2*, and *slc9a3* increased 2.2-, 2.8-, and 2-fold, respectively, after 2 wk of HA-SW exposure (Fig. 7, B, C, E). In contrast, *slc9a2* decreased about 34% after HA-SW exposure (Fig. 7D).

DISCUSSION

The noninvasive SIET was previously applied to reveal acid (H⁺) secretion by yolk-sac ionocytes in zebrafish (9, 29) and

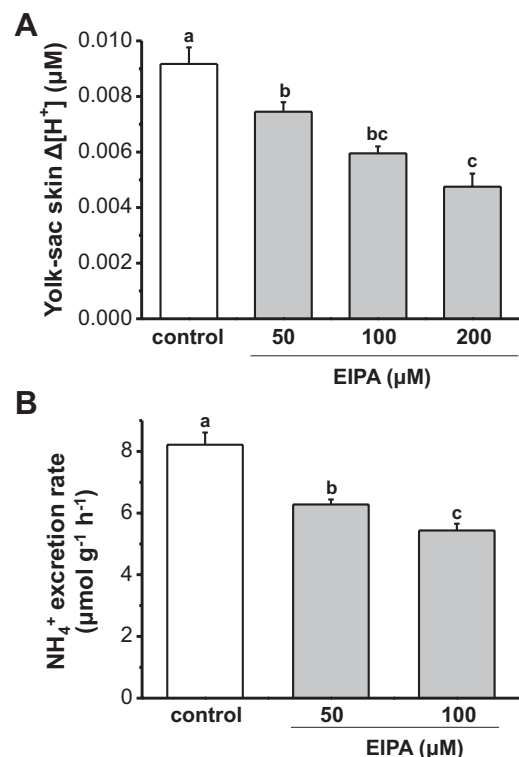


Fig. 5. Effects of EIPA on $\Delta[\text{H}^+]$ at the yolk sac surface (A) and ammonia excretion rates (B) of larvae acclimated to seawater ($n = 9$ individuals for $\Delta[\text{H}^+]$; $n = 5$ for the ammonia excretion rate). Data are presented as the means \pm SE. ^{a,b,c}Different letters indicate a significant difference (one-way ANOVA, Tukey's comparison, $P < 0.05$).

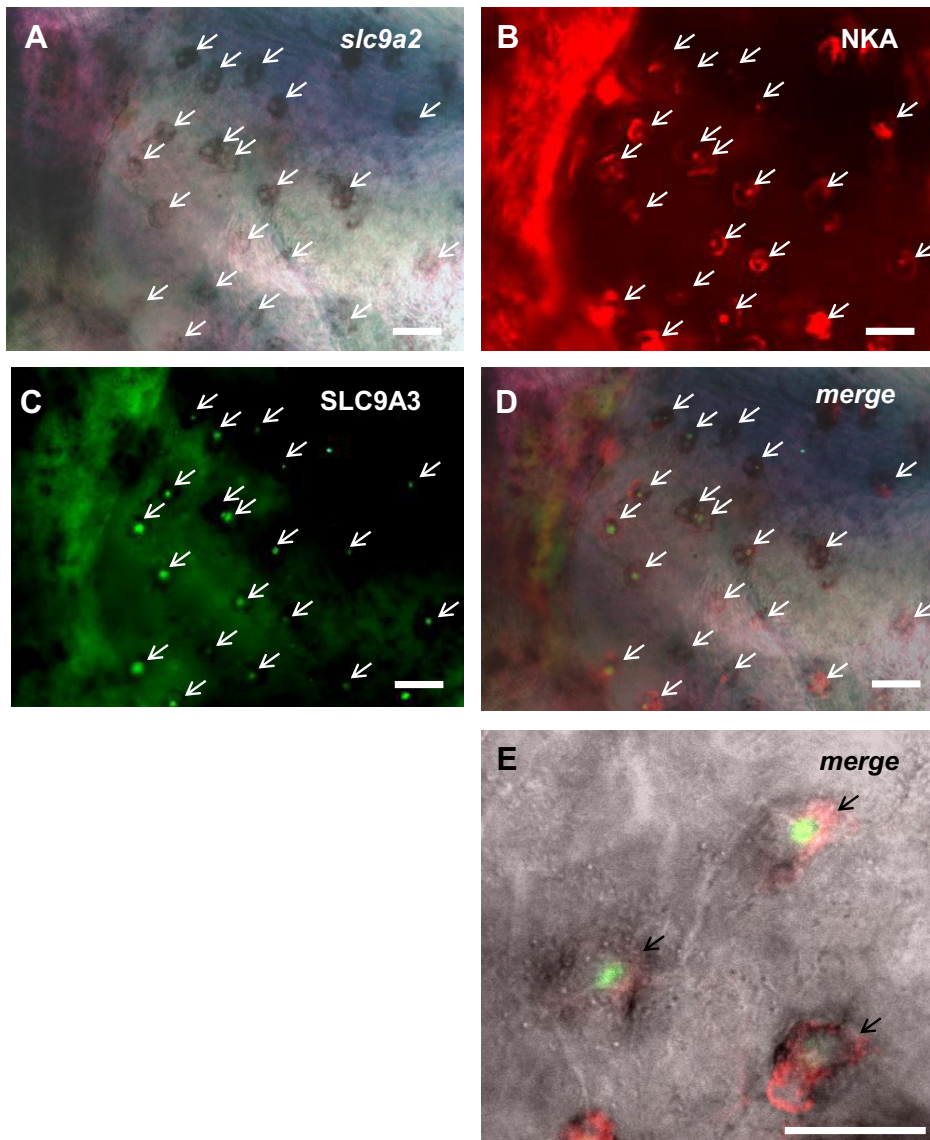


Fig. 6. Localization of *slc9a2* (NHE2) and *slc9a3* (NHE3) in yolk-sac ionocytes of seawater-acclimated larvae. *A*: *slc9a2* in situ hybridization. *B*: NKA immunohistochemistry. *C*: *slc9a3* immunohistochemistry. *D* and *E*: merged images of *A*–*C*. Arrows indicate ionocytes. Scale bars in *A*–*D* are 10 μm . Scale bar in *E* is 100 μm .

FW-acclimated medaka (18, 40). Herein, we used the same approach to show that ionocytes secrete H^+ to acidify the yolk sac surface of medaka larva in SW. The H^+ gradient at the yolk sac surface was even larger in SW-acclimated larvae than in FW-acclimated larvae (both SW and FW were adjusted to pH 8; Fig. 2*B*). Because the buffering capacity of SW is higher than that of FW, it is obvious that a medaka larva secretes more acid in SW than in FW. In SW, the H^+ gradient measured at the surface of ionocytes was remarkably higher than that of keratinocytes, reflecting the critical role of ionocytes in acid secretion.

Interestingly, alkalization of the yolk-sac surface (including both ionocyte and keratinocyte surfaces) occurred in larvae acclimated to HA-SW (Fig. 2, *B* and *C*), suggesting that accumulated ammonia was released onto the cell surface, mostly as nonionic NH_3 , which consumed the accumulated acid. In contrast, if ammonia were released as mostly NH_4^+ , acidification of skin surface would have been detected. A similar phenomenon was also found in zebrafish and medaka larvae in FW (29, 40). When using Tricine buffer to eliminate

the acid layer, the NH_4^+ excretion rate of larvae was significantly suppressed (Fig. 4), also supporting nonionic NH_3 being excreted by SW medaka and the proton-facilitated ammonia excretion.

In this study, we attempted to measure the NH_4^+ gradient with the SIET but found that the selectivity of the microelectrode for NH_4^+ was poor in SW medium; therefore, SW larvae were acutely transferred to FW medium for NH_4^+ recording. The result (Fig. 3*A*) showed positive NH_4^+ gradient at both ionocytes and keratinocytes, and the gradients were remarkably higher at ionocytes than at keratinocytes, suggesting ammonia excretion by both cell types. However, it should be noted that the FW transfer might influence the mechanism of ammonia excretion, and the measured NH_4^+ gradient may not reflect the true gradient in SW. In addition to the SIET data, a conventional ammonia assay with an enzyme reaction was also used to determine the whole-larval NH_4^+ excretion rate in SW (Fig. 3*B*). No significant difference was found in NH_4^+ excretion rates between FW- and SW-acclimated larvae, suggesting that ammonia excretion in medaka larvae is not affected by salinity.

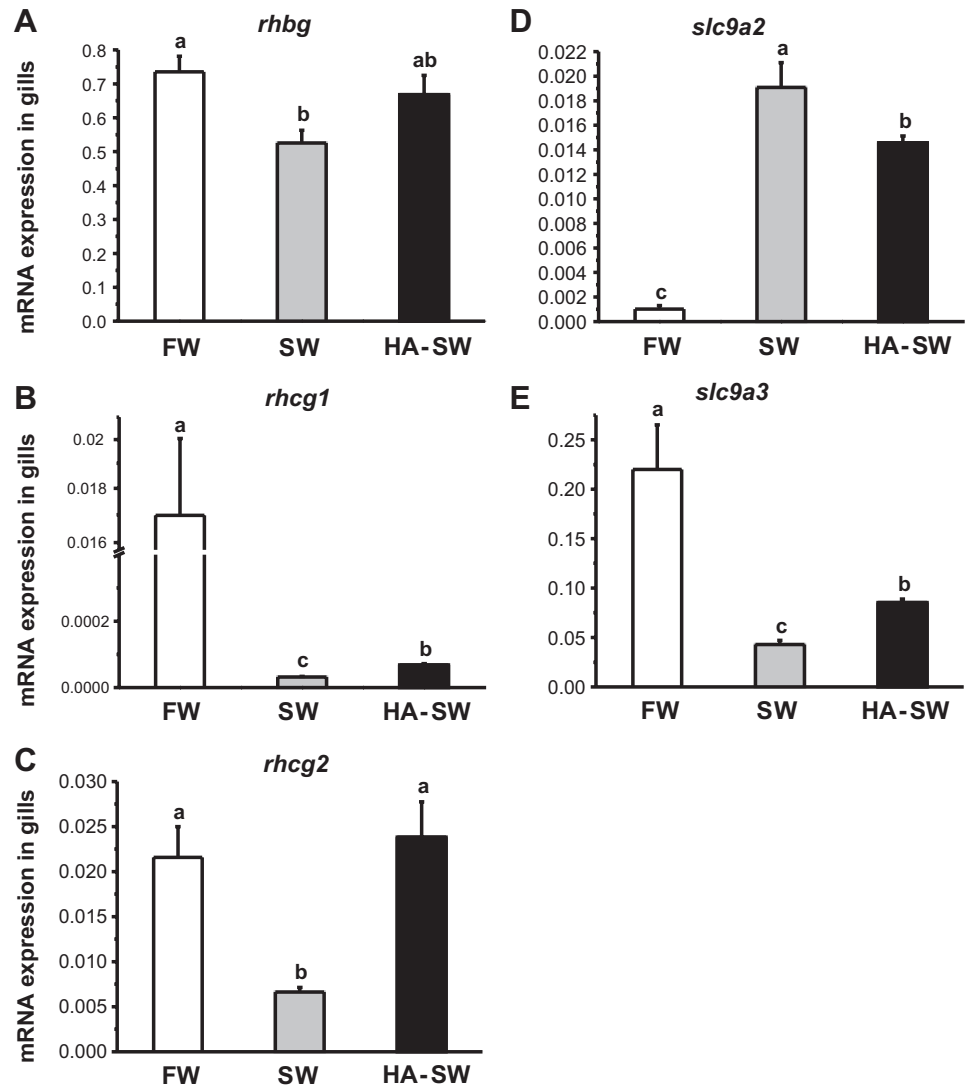


Fig. 7. mRNA expressions of *rhbg* (A), *rhcg1* (B), *rhcg2* (C), *slc9a2* (D), and *slc9a3* (E) in gills of medaka acclimated to FW and SW, and HA-SW for 2 wk. Data are presented as the means \pm SE; $n = 5$. ^{a,b,c}Different letters indicate a significant difference (one-way ANOVA, Tukey's comparison, $P < 0.05$).

The effect of salinity on ammonia excretion seems to be inconsistent among fish species. An increase in salinity did not alter the ammonia excretion rate in toadfish (*Allenbatrachus grunniens*) (2, 33) but decreased it in gulf sturgeon (*Acipenser oxyrinchus desotoi*) and striped bass (*Morone saxatilis*) (1). Whereas an increase in salinity was found to stimulate ammonia excretion in Atlantic salmon (*Salmo salar*) (17) and mangrove killifish (*Rivulus marmoratus*) (8), in a recent study on rainbow trout, the net ammonia efflux rate was higher in SW than in FW-acclimated individuals (37).

In zebrafish larvae, both H^+ -ATPase and the Na^+/H^+ exchanger (NHE3) in apical membranes contribute to H^+ secretion by yolk-sac ionocytes (HR cells) (11). However, in the case of medaka acclimated to FW, only NHE3 was found in apical membranes of ionocytes (40); H^+ -ATPase was found in basolateral membranes of a minor population of ionocytes but did not contribute to H^+ secretion (18). In SW-acclimated medaka, H^+ -ATPase was not detected in ionocytes by IHC (data not shown). In addition, EIPA treatment significantly suppressed the H^+ gradient, demonstrating the role of NHE in secreting acid into SW (Fig. 5A). Because the high Na^+ concentration of SW favors the

driving of NHE in apical membranes of ionocytes, this could be the reason why acid secretion was greater in SW than FW (Fig. 2B). It is generally accepted that SW fish excrete metabolic acid via the NHE but not H^+ -ATPase in apical membranes of ionocytes (3, 5, 11). In several studies, the molecular identity and cellular localization of NHE isoforms in marine and euryhaline fishes were reported. In the stingray (*Dasyatis sabina*) and dogfish (*Squalus acanthias*), NHE3 or NHE2 was identified in apical membranes of gill ionocytes (3, 6). Using heterologous antibodies (against mammalian NHE2), Edwards et al. (6) demonstrated the colocalization of NHE2 and NKA in gills of several elasmobranch species. In a marine teleost, *Myoxocephalus octodecemspinosus*, NHE2 was also found in apical membranes of gill ionocytes (3). However, those studies did not report if the two NHE isoforms (NHE2 and NHE3) were expressed by the same ionocytes. In this study, we used in situ hybridization and IHC to show for the first time that both *NHE2* (mRNA) and NHE3 (protein) are expressed by the same SW ionocytes (Fig. 6). Similar distributions of NHE2 and NHE3 were found in FW ionocytes (PNA⁺ cells) of rainbow trout (15).

Although both NHE2 and NHE3 were expressed by the same ionocytes, their regulations differed. The mRNA expression of NHE3 was downregulated, but that of NHE2 was upregulated in gills of medaka subjected to SW acclimation (Fig. 7). The mRNA level of NHE2 was roughly equivalent to that of NHE3 in SW, indicating that both NHE2 and NHE3 are required in SW. Interestingly, reverse regulation of NHE2 and NHE3 was revealed in SW medaka exposed to HA water (Fig. 8). NHE3 was upregulated by HA exposure, whereas NHE2 was downregulated. Similar results were reported in pufferfish exposed to HA (25). The upregulation of NHE3 suggests that

NHE3 is associated with ammonia excretion in SW. Meanwhile, the downregulation of NHE2 might maintain a balance between the two isoforms in acid secretion. On the other hand, the two isoforms might perform different kinetics and properties for specific kind of roles. In mammalian kidneys, the major distributions of NHE2 and NHE3 are in Henle's loop and the proximal convoluted tubule, respectively (4, 27). Kinetic studies showed that the affinities to H^+ and Na^+ were higher in NHE3 than in NHE2 (26, 41), suggesting that NHE2 is more suitable for working in a high extracellular Na^+ environment (renal medulla). For a better understanding of the role of the two NHE isoforms in ionocytes, it is necessary to examine their kinetics in the future.

NHE has long been speculated to function as a Na^+/NH_4^+ exchanger based on the observation that ammonia excretion can be suppressed by NHE inhibitors (28, 36, 38). We cannot rule out this possibility until a functional characterization of fish NHE is achieved. However, if this speculation is true for FW or SW fish, proton-facilitated ammonia excretion by ionocytes would be unlikely, and it would conflict with the coupling model of NHE3 and Rhcg1 in medaka (40) because NH_4^+ excretion via NHE3 does not favor the driving of NH_3 diffusion via Rhcg1 and would even cause back-flux via Rhcg1.

Localization of *Rhcg1* and *Rhbg* mRNA with in situ hybridization showed that they are colocalized in the same ionocytes of FW-acclimated medaka larvae (40). However, their localizations in SW ionocytes were not successful in this study, probably because of their low expression level in SW ionocytes. Real-time PCR data showed that expressions of these Rh genes (*Rhbg*, *Rhcg1*, and *Rhcg2*) were downregulated in SW but upregulated in HA (Fig. 7), suggesting that Rh glycoproteins are still required for excreting ammonia into SW. Since the NH_4^+ excretion rate did not differ between FW- and SW-acclimated larvae (Fig. 3B), downregulation of Rh glycoproteins in SW might reflect another ammonia excretion pathway being induced and/or the efficiency of Rh protein-mediated ammonia excretion being enhanced. Since the high Na^+ concentration of SW favors the driving of NHE, elevated H^+ secretion probably promotes NH_3 diffusion via Rh proteins. In contrast to the tight nature of the gill epithelium in FW fish, junctions between ionocytes and accessory cells of SW fish are relatively leaky (16, 21). Therefore, NH_4^+ (NH_3) excretion via a paracellular pathway might be another pathway in SW fish.

In our previous studies, coupling of NHE3 and Rhcg1 was suggested to mediate Na^+ uptake, and acid and ammonia excretion by ionocytes of medaka in FW (18, 40). Low- Na^+ water (40), acidic water (18), and HA water (unpublished data) were found to upregulate both NHE3 and Rhcg1. In this study, NHE3 and Rhcg1 were both downregulated in SW and upregulated in HA, suggesting that the roles of NHE3 and Rhcg1 in SW medaka are similar to those in FW medaka. As proposed in FW medaka (18, 40), NHE3 transports H^+ out of ionocytes, and the accumulated surface H^+ further traps the NH_3 that diffuses across Rhcg1. In addition to NHE3, NHE2 might also contribute to H^+ secretion in SW ionocytes, but it might not physically join with Rhcg1 in apical membranes. Further investigation of this speculation is required.

In addition to NHE and Rh glycoproteins, other transporters and enzymes were suggested to transport ammonia. In the euryhaline climbing perch (*Anabas testudineus*), gill mRNA

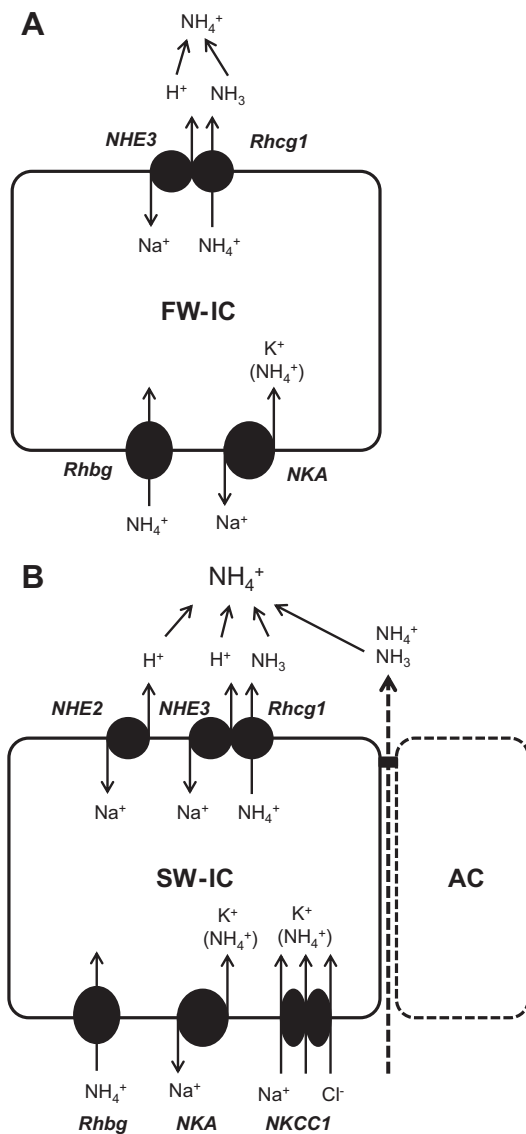


Fig. 8. A putative model of ammonia excretion by freshwater-type ionocytes (FW-IC) and seawater-type ionocytes (SW-IC) of medaka. The Na^+-H^+ exchanger (NHE3) and Rhcg1 mediate the proton-facilitated ammonia excretion in the apical membrane of FW-IC; in the basolateral membrane, Rhbg and $Na^+-K^+-ATPase$ (NKA) carry NH_4^+ into ionocytes (A) (39). In the apical membrane of SW-IC, both NHE2 and NHE3 secrete H^+ to trap the NH_3 moved through Rhcg1 and a paracellular pathway; in the basolateral membrane, $Na^+-K^+-ATPase$ (NKA), $Na^+-K^+-2Cl^-$ cotransporter (NKCC1), and Rhbg carry NH_4^+ into ionocytes. In addition, NH_4^+ also diffuses out of fish through leaky junctions (the paracellular pathway) between SW-IC and adjacent accessory cells (AC).

levels of $\text{Na}^+\text{-K}^+\text{-ATPase}$ (NKA), $\text{Na}^+\text{-K}^+\text{-2Cl}^-$ cotransporter (NKCC1), and CFTR Cl^- channel were induced by high ammonia exposure, suggesting that they are involved in ammonia excretion by SW-type ionocytes (13, 14, 20). In a recent study, NKA and NKCC1 were colocalized to the basolateral membrane of SW ionocyte in medaka larvae (22). Taken all of the evidence together, a putative model of ammonia excretion by SW and FW ionocytes of medaka is proposed (Fig. 8).

In conclusion, this study provides molecular and physiological evidence to show that ionocytes play a role in acid and ammonia excretion of SW medaka. Ammonia excretion in SW medaka is facilitated by proton secretion of ionocytes in which NHE and Rh glycoproteins are involved.

ACKNOWLEDGMENTS

This work was supported by a National Science Council of Taiwan Research grants to L. Y. Lin and J. L. Horng.

DISCLOSURES

No conflicts of interest, financial or otherwise, are declared by the authors.

AUTHOR CONTRIBUTIONS

Author contributions: S.-T.L., L.T., J.-L.H., and L.-Y.L. conception and design of research; S.-T.L., L.T., J.-L.H., and L.-Y.L. performed experiments; S.-T.L., L.T., J.-L.H., and L.-Y.L. analyzed data; S.-T.L., J.-L.H., and L.-Y.L. interpreted results of experiments; S.-T.L., J.-L.H., and L.-Y.L. prepared figures; S.-T.L., J.-L.H., and L.-Y.L. drafted manuscript; J.-L.H. and L.-Y.L. edited and revised manuscript; J.-L.H. and L.-Y.L. approved final version of manuscript.

REFERENCES

- Altinok I, Grizzle JM. Excretion of ammonia and urea by phylogenetically diverse fish species in low salinities. *Aquaculture* 238: 499–507, 2004.
- Barimo JF, Steele SL, Wright PA, Walsh PJ. Dogmas and controversies in the handling of nitrogenous wastes: ureotely and ammonia tolerance in early life stages of the gulf toadfish, *Opsanus beta*. *J Exp Biol* 207: 2011–2020, 2004.
- Catches JS, Burns JM, Edwards SL, Claiborne JB. Na^+/H^+ antiporter, $\text{V-H}^+\text{-ATPase}$ and $\text{Na}^+/\text{K}^+\text{-ATPase}$ immunolocalization in a marine teleost (*Myoxocephalus octodecemspinosus*). *J Exp Biol* 209: 3440–3447, 2006.
- Chambrey R, Warnock DG, Podevin RA, Bruneval P, Mandet C, Bélair MF, Bariéty J, MP. Immunolocalization of the Na^+/H^+ exchanger isoform NHE2 in rat kidney. *Am J Physiol Renal Physiol* 275: F379–F386, 1998.
- Claiborne JB, Heisler N. Acid-base regulation and ion transfers in the carp (*Cyprinus carpio*): pH compensation during graded long- and short-term environmental hypercapnia, and the effect of bicarbonate infusion. *J Exp Biol* 126: 41–61, 1986.
- Edwards SL, Donald JA, Toop T, Donowitz M, Tse CM. Immunolocalisation of sodium/proton exchanger-like proteins in the gills of elasmobranchs. *Comp Biochem Physiol A Mol Integr Physiol* 131: 257–265, 2002.
- Evans DH, Piermarini PM, Choe KP. The multifunctional fish gill: dominant site of gas exchange, osmoregulation, acid-base regulation, and excretion of nitrogenous waste. *Physiol Rev* 85: 97–177, 2005.
- Frick NT, Wright PA. Nitrogen metabolism and excretion in the mangrove killifish *Rivulus marmoratus* II. Significant ammonia volatilization in a teleost during air-exposure. *J Exp Biol* 205: 91–100, 2002.
- Horng JL, Lin LY, Hwang PP. Functional regulation of $\text{H}^+\text{-ATPase}$ -rich cells in zebrafish embryos acclimated to an acidic environment. *Am J Physiol Cell Physiol* 296: C682–C692, 2009.
- Hung CY, Tsui KN, Wilson JM, Nawata CM, Wood CM, Wright PA. Rhesus glycoprotein gene expression in the mangrove killifish *Kryptolebias marmoratus* exposed to elevated environmental ammonia levels and air. *J Exp Biol* 210: 2419–2429, 2007.
- Hwang PP, Lee TH, Lin LY. Ion regulation in fish gills: recent progress in the cellular and molecular mechanisms. *Am J Physiol Regul Integr Comp Physiol* 301: R28–R47, 2011.
- Ip YK, Chew SF. Ammonia production, excretion, toxicity, and defense in fish: a review. *Front Physiol* 1: 134, 2010.
- Ip YK, Loong AM, Kuah JS, Sim EW, Chen XL, Wong WP, Lam SH, Delgado IL, Wilson JM, Chew SF. Roles of three branchial $\text{Na}^+\text{-K}^+\text{-ATPase}$ α -subunit isoforms in freshwater adaptation, seawater acclimation, and active ammonia excretion in *Anabas testudineus*. *Am J Physiol Regul Integr Comp Physiol* 303: R112–R125, 2012.
- Ip YK, Wilson JM, Loong AM, Chen XL, Wong WP, Delgado IL, Lam SH, Chew SF. Cystic fibrosis transmembrane conductance regulator in the gills of the climbing perch, *Anabas testudineus*, is involved in both hypoosmotic regulation during seawater acclimation and active ammonia excretion during ammonia exposure. *J Comp Physiol B* 182: 793–812, 2012.
- Ivanis G, Esbaugh AJ, Perry SF. Branchial expression and localization of SLC9A2 and SLC9A3 sodium/hydrogen exchangers and their possible role in acid-base regulation in freshwater rainbow trout (*Oncorhynchus mykiss*). *J Exp Biol* 211: 2467–2477, 2008.
- Karnaky KJ Jr, Degnan KJ, Garretson LT, Zadunaisky JA. Identification and quantification of mitochondria-rich cells in transporting epithelia. *Am J Physiol Regul Integr Comp Physiol* 246: R770–R775, 1984.
- Knoph MB, Olsen YA. Subacute toxicity of ammonia to Atlantic salmon (*Salmo salar* L.) in seawater: effects on water and salt balance, plasma cortisol and plasma ammonia levels. *Aquat Toxicol (Amst)* 30: 295–310, 1994.
- Lin CC, Lin LY, Hsu HH, Thermes V, Prunet P, Horng JL, Hwang PP. Acid secretion by mitochondrion-rich cells of medaka (*Oryzias latipes*) acclimated to acidic freshwater. *Am J Physiol Regul Integr Comp Physiol* 302: R283–R291, 2012.
- Lin LY, Horng JL, Kunkel JG, Hwang PP. Proton pump-rich cell secretes acid in skin of zebrafish larvae. *Am J Physiol Cell Physiol* 290: C371–C378, 2006.
- Loong AM, Chew SF, Wong WP, Lam SH, Ip YK. Both seawater acclimation and environmental ammonia exposure lead to increases in mRNA expression and protein abundance of $\text{Na}^+:\text{K}^+:\text{2Cl}^-$ cotransporter in the gills of the climbing perch, *Anabas testudineus*. *J Comp Physiol B* 182: 491–506, 2012.
- Marshall WS. Transport processes in isolated teleost epithelia: opercular epithelium and urinary bladder. In: *Cellular and Molecular Approaches in Fish Ionic Regulation: Fish Physiology*, edited by Wood CM and Shuttleworth TJ. vol. 14, San Diego, CA: Academic, 1995, p. 1–23.
- Miyaniishi H, Okubo K, Kaneko T, Takei Y. Role of cardiac natriuretic peptides in seawater adaptation of medaka embryos as revealed by loss-of-function analysis. *Am J Physiol Regul Integr Comp Physiol* 304: R423–R434, 2013.
- Nakada T, Hoshijima K, Esaki M, Nagayoshi S, Kawakami K, Hirose S. Localization of ammonia transporter Rhcg1 in mitochondrion-rich cells of yolk sac, gill, and kidney of zebrafish and its ionic strength-dependent expression. *Am J Physiol Regul Integr Comp Physiol* 293: R1743–R1753, 2007.
- Nakada T, Westhoff CM, Kato A, Hirose S. Ammonia secretion from fish gill depends on a set of Rh glycoproteins. *FASEB J* 21: 1067–1074, 2007.
- Nawata CM, Hirose S, Nakada T, Wood CM, Kato A. Rh glycoprotein expression is modulated in pufferfish (*Takifugu rubripes*) during high environmental ammonia exposure. *J Exp Biol* 213: 3150–3160, 2010.
- Orlowski J. Heterologous expression and functional properties of amiloride high-affinity (NHE-1) and low-affinity (NHE-3) isoforms of the rat Na/H exchanger. *J Biol Chem* 268: 16369–16377, 1993.
- Orlowski J, Grinstein S. Diversity of the mammalian sodium/proton exchanger SLC9 gene family. *Eur J Physiol* 447: 549–565, 2004.
- Payan P. A study of the $\text{Na}^+/\text{NH}_4^+$ exchange across the gill of the perfused head of the trout (*Salmo gairdneri*). *J Comp Physiol A* 124: 181–188, 1978.
- Shih TH, Horng JL, Hwang PP, Lin LY. Ammonia excretion by the skin of zebrafish (*Danio rerio*) larvae. *Am J Physiol Cell Physiol* 295: C1625–C1632, 2008.
- Shih TH, Horng JL, Liu ST, Hwang PP, Lin LY. Rhcg1 and NHE3b are involved in ammonium-dependent sodium uptake by zebrafish larvae acclimated to low-sodium water. *Am J Physiol Regul Integr Comp Physiol* 302: R84–R93, 2012.

31. **Sohet F, Colin Y, Genetet S, Ripoche P, Metral S, Kim CLV, Lopez C.** Phosphorylation and ankyrin-G binding of the C-terminal domain regulate targeting and function of the ammonium transporter RhBG. *J Biol Chem* 283: 26557–26567, 2008.
32. **Wagner CA, Devuyst O, Belge H, Bourgeois S, Houillier P.** The rhesus protein RhCG: a new perspective in ammonium transport and distal urinary acidification. *Kidney Int* 79: 154–161, 2011.
33. **Walsh PJ, Wei Z, Wood CM, Loong AM, Hiong KC, Lee SM, Wong WP, Chew SF, Ip YK.** Nitrogen metabolism and excretion in *Allenbatrachus grunniens* (L): effects of variable salinity, confinement, high pH and ammonia loading. *J Fish Biol* 65: 1392–1411, 2004.
34. **Weihrauch D, Wilkie MP, Walsh PJ.** Ammonia and urea transporters in gills of fish and aquatic crustaceans. *J Exp Biol* 212: 1716–1730, 2009.
35. **Wilkie MP.** Ammonia excretion and urea handling by fish gills: present understanding and future research challenges. *J Exp Zool* 293: 284–301, 2002.
36. **Wilson RW, Wright PM, Munger S, Wood CM.** Ammonia excretion in freshwater rainbow trout (*Oncorhynchus mykiss*) and the importance of gill boundary layer acidification: lack of evidence for $\text{Na}^+/\text{NH}_4^+$ exchange. *J Exp Biol* 191: 37–58, 1994.
37. **Wood CM, Nawata CM.** A nose-to-nose comparison of the physiological and molecular responses of rainbow trout to high environmental ammonia in seawater versus freshwater. *J Exp Biol* 214: 3557–3569, 2011.
38. **Wright PA, Wood CM.** An analysis of branchial ammonia excretion in the freshwater rainbow trout: effects of environmental pH change and sodium uptake blockade. *J Exp Biol* 114: 329–353, 1985.
39. **Wright PA, Wood CM.** A new paradigm for ammonia excretion in aquatic animals: role of Rhesus (Rh) glycoproteins. *J Exp Biol* 212: 2303–2312, 2009.
40. **Wu SC, Horng JL, Liu ST, Hwang PP, Wen ZH, Lin CS, Lin LY.** Ammonium-dependent sodium uptake in mitochondrion-rich cells of medaka (*Oryzias latipes*) larvae. *Am J Physiol Cell Physiol* 298: C237–C250, 2010.
41. **Yu FH, Shull GE, Orlowski J.** Functional properties of the rat Na/H exchanger NHE-2 isoform expressed in Na/H exchanger-deficient Chinese hamster ovary cells. *J Biol Chem* 268: 25536–25541, 1993.

